Expanding the Reach of RNAi Therapeutics with Next Generation Lipophilic siRNA Conjugates

Kirk Brown
Alnylam Pharmaceuticals
Jayaprakash Nair
Alnylam Pharmaceuticals
Maja Janas
Alnylam Pharmaceuticals
Yesseinia Anglero-Rodriguez
Alnylam Pharmaceuticals
Haiyan Peng
Alnylam Pharmaceuticals
Christopher Theile
Alnylam Pharmaceuticals
Elena Castellanos-Rizaldos
Alnylam Pharmaceuticals
Christopher Brown
Alnylam Pharmaceuticals
Donald Foster
Alnylam Pharmaceuticals
Jeffrey Kurz
Alnylam Pharmaceuticals
Jeffrey Allen
Alnylam Pharmaceuticals
Raj Maganti
Alnylam Pharmaceuticals
Jing Li
Alnylam Pharmaceuticals https://orcid.org/0000-0002-2414-8523
Shigeo Matsuda
Alnylam Pharmaceuticals
Tyler Chickering
Alnylam Pharmaceuticals
Michelle Jung
Alnylam Pharmaceuticals
Kelly Wassarman

Alnylam Pharmaceuticals
Jeff Rollins
Alnylam Pharmaceuticals
Lauren Woods Lauren Woods
Alnylam Pharmaceuticals
Alex Kelin
Alnylam Pharmaceuticals
Dale Gunther
Alnylam Pharmaceuticals
Melissa Mobley
Alnylam Pharmaceuticals
John Petrulis
Alnylam Pharmaceuticals
Robin McDougall
Alnylam Pharmaceuticals
Tim Racie
Alnylam Pharmaceuticals
Jessica Bombardier
Alnylam Pharmaceuticals
Diana Cha
Alnylam Pharmaceuticals
Saket Agarwal
Alnylam Pharmaceuticals
Lei Johnson
Alnylam Pharmaceuticals
Yongfeng Jiang
Alnylam Pharmaceuticals
Scott Lentini
Alnylam Pharmaceuticals
Jason Gilbert
Alnylam Pharmaceuticals
Tuyen Nguyen
Alnylam Pharmaceuticals
Samantha Chigas
Alnylam Pharmaceuticals
Sarah Le Blanc Sarah Le Blanc
Alnylam Pharmaceuticals
Urjana Poreci
Alnylam Pharmaceuticals

Anne Kasper
Alnylam Pharmaceuticals
Arlin Rogers
Alnylam Pharmaceuticals
Saeho Chong
Alnylam Pharmaceuticals
Wendell Davis
Alnylam Pharmaceuticals
Jessica Sutherland
Alnylam Pharmaceuticals
Adam Castoreno
Alnylam Pharmaceuticals
Stuart Milstein
Alnylam Pharmaceuticals
Mark Schlegel
Alnylam Pharmaceuticals https://orcid.org/0000-0002-0127-608X
Ivan Zlatev
Alnylam Pharmaceuticals https://orcid.org/0000-0003-2797-3032
Klaus Charisse
Alnylam Pharmaceuticals
Mark Keating
Alnylam Pharmaceuticals
Muthiah Manoharan
Alnylam
Kevin Fitzgerald
Jing-Tao Wu
Alnylam
Martin Maier
Alnylam Pharmaceuticals (United States)
Vasant Jadhav (**vjadhav@alnylam.com**)
Alnylam Pharmaceuticals

Article

Keywords: RNAi therapeutics, drug delivery, silencing, gene transcripts

Posted Date: October 21st, 2021

DOI: https://doi.org/10.21203/rs.3.rs-946835/v1

Version of Record: A version of this preprint was published at Nature Biotechnology on June 2nd, 2022.
See the published version at https://doi.org/10.1038/s41587-022-01334-x.

Abstract

RNA interference (RNAi) therapeutics are a new class of medicines that can address unmet medical needs by silencing disease-causing gene transcripts. While delivery of short interfering RNAs (siRNAs) to hepatocytes has yielded multiple drug approvals, novel delivery solutions are needed to expand the reach of RNAi therapeutics. Here we report that conjugation of 2'-*O*-hexadecyl (C16) to siRNAs enables efficient silencing in the central nervous system (CNS), eye, and lung of multiple nonclinical species with broad cell type specificity. Intrathecally delivered C16-siRNAs are active across CNS regions and cell types, with sustained silencing for at least three months, which is an especially important outcome considering the challenging dosing route. Similarly, intravitreal and intranasal administration of C16-siRNAs resulted in potent and sustained knockdown in the eye and lung, respectively. Efficient delivery facilitated through C16 conjugation to optimized siRNA designs has enabled candidate selection for investigational human clinical trials assessing therapeutic silencing beyond the liver with infrequent (e.g. bi-annual) dosing.

Introduction

RNA interference (RNAi) therapeutics utilize an endogenous mechanism whereby short interfering RNAs (siRNAs) direct the RNA-induced silencing complex (RISC) to target gene transcripts, resulting in a sequence-specific and catalytic RNA cleavage and subsequent lowering of the target protein[1]. To confer drug-like properties, siRNAs are chemically modified to increase nuclease resistance and minimize immune recognition. Intracellular delivery of these siRNAs is enabled through nanoparticle formulation or ligand conjugation. For liver targets, lipid nanoparticles (LNPs) and N-acetylgalactosamine (GalNAc) conjugates are two clinically validated delivery strategies, with multiple regulatory approvals that include Onpattro® (patisiran)[2,3], Givlaari® (givosiran)[4], Oxlumo® (lumaisran)[5], and Leqvio® (inclisiran)[6–8], and numerous additional programs in various stages of clinical development across several therapeutic areas.

The naturally occurring RNAi pathway can also be harnessed in extrahepatic organs by building on nearly two decades of efforts on liver siRNA design optimization[9–12]; however, novel delivery approaches are needed. Such organs include the central nervous system (CNS), eye, and lung that can be accessed by local, albeit challenging, delivery. Diseases of the CNS represent some of the highest unmet medical needs and greatest therapeutic challenges. Multiple CNS diseases have been associated with dominant mutations, making them suitable candidates for an RNAi-based silencing approach. While one antisense oligonucleotide (ASO), Spinraza® (nusinersen), has been approved for the treatment of spinal muscular atrophy[13], the potential of siRNAs to treat CNS diseases such as chronic neuropathic pain[14], Machado-Joseph disease[15], HIV-1 encephalopathy[16], and Huntington's disease[17,18] has only been explored preclinically with central administration into the cerebrospinal fluid (CSF) or directly into the brain parenchyma. Accessing the CNS broadly, effectively, and safely remains challenging. Recently, chemically modified siRNA scaffolds demonstrated potent and sustained silencing in rodents and nonhuman

primates (NHPs) after administration into CSF[19]. Technologies enabling siRNA delivery across the blood brain barrier following less challenging systemic administration are also being explored[20–22].

In addition to CNS, infrequent delivery of metabolically stabilized siRNAs directly into the eye has several benefits, including increased bioavailability compared to systemic administration, greater patient adherence, reduced health care burden, and fewer side effects such as elevated risk of developing cataracts, retinal detachment, endophthalmitis, and vitreous hemorrhage compared to other therapeutic modalities that require more frequent administration. The safety and efficacy of at least nine siRNAs has been evaluated in humans following intravitreal (IVT) or topical administration. Fully unmodified and partially chemically modified siRNA designs were evaluated in the late stage clinical studies and none have been terminated due to safety concerns[23]. The first therapeutic application of siRNAs in the eye was for the treatment of wet age-related macular degeneration in 2004, and since then many additional ocular indications have been explored, including glaucoma, dry eye, diabetic macular edema, retinitis pigmentosa, Usher syndrome, and non-arteritic anterior ischemic optic neuropathy.

Local delivery of siRNAs into the lung allows rapid drug access to the respiratory tissues on the airside of the lung. Intranasal (IN), intratracheal, and inhaled administration of oligonucleotides has been explored preclinically and clinically for the treatment of the respiratory syncytial virus[24], cystic fibrosis[25], idiopathic pulmonary fibrosis[26] and other lung diseases. Furthermore, the pandemic of COVID-19 highlighted the importance of enabling siRNA delivery to the lung for the treatment of emergent viral respiratory diseases.

Here, we describe combining 2'-*O*-hexadecyl (C16) conjugation with metabolically stable siRNAs, featuring full modification of the 2'-position of the ribose and strategically placed phosphorothioate (PS) linkages, to enable delivery into the CNS, eye, and lung resulting in robust and long-lasting gene silencing in rodents and NHPs. Our results indicate that C16-siRNAs administered via a clinically feasible intrathecal (IT) route of administration have durable activity across CNS regions and cell types, with a favorable nonclinical safety profile to date. We also demonstrate that the C16-siRNA platform enables durable silencing after IVT delivery into the eye and via IN delivery into the lung. The long durability of RNAi technology will be particularly beneficial to patients by potentially lessening the frequency of IT and IVT dose administration. We believe that these advances have the potential to generate multiple candidates for investigating safety and efficacy in humans.

Results

Optimization of the siRNA design for CNS delivery

Lipophilic moieties represent one of the earliest approaches employed to improve cellular uptake and delivery of ASOs and siRNAs to the liver and various other organ systems including the CNS[27-29]. Based on internal and reported data, we rationalized that by carefully optimizing the lipophilicity of our chemically modified siRNAs, we could enhance intracellular delivery without compromising broad biodistribution and safety. Further, we decided to utilize the 2'-position of the ribose sugar backbone to

introduce the lipophilic moiety as it provides numerous options for the positioning of the lipophile in the siRNA duplex.

First, the impact of lipophile chain length was evaluated in rat CNS utilizing a Superoxide Dismutase 1 (SOD1)-targeting siRNA featuring an Enhanced Stabilization Chemistry (ESC) design (Supplementary Table 1). For this study, the lipophile was introduced at the N6 (position 6 from 5'-end) of the sense strand which was previously shown to tolerate large 2'-substituents (unpublished data). RNAi activity in the CNS generally increased with lipid chain length, with 2'-*O*-C16 providing optimal activity in the rat spinal cord and brain at two weeks after a single IT dose of 0.9 mg (Fig. 1a). To determine the positional impact of 2'-*O*-C16 conjugation on siRNA potency and to confirm sense strand N6 as one of the preferred conjugation sites, 2'-*O*-C16 was walked across both the sense and antisense strands of the SOD1 siRNA, and the resulting compounds were screened for inherent activity via transfection in RPE-J cells (Fig.1b). 2'-*O*-C16 was well tolerated across both strands, with potency similar to the unconjugated siRNA, except for a few positions known to be sensitive to sterically demanding 2'-modifications[9]. As expected, 2'-*O*-C16 conjugation was not well tolerated at sense strand N9-11 which is in the region cleaved by Ago2 during functional RISC formation and known to be sensitive to bulky 2'-modifications. A subset of the C16-siRNAs was selected for in vivo evaluation in rats. One month after a single 0.9 mg IT dose, most tested positions provided activity equivalent to sense strand N6 (Fig. 1c), confirming tolerance of 2'-*O*-C16 modification at multiple positions of the siRNA sense strand.

Next, we evaluated other siRNA design elements and confirmed that full chemical modification with strategic placement of 2'-fluoro and 2'-*O*-methyl modifications[9] is required for robust siRNA activity in the CNS. Furthermore, the ESC+ chemistry employing glycol nucleic acid (GNA) in the antisense seed region for increased specificity[10,30] retained activity in rat two weeks after a single 0.9 mg IT dose (Fig. 1d). The relative importance of 2'-*O*-C16 and 5'-(*E*)-vinylphosphonate (VP), a 5' phosphate mimic placed at the 5'-end of the antisense strand to promote RISC loading[31], was assessed utilizing the ESC SOD1-targeting siRNA in rats. At one month post a single IT dose of 0.9 mg, an unconjugated siRNA with no 5'-VP had minimal activity in the spinal cord and brain (Fig. 1e). The addition of either 5'-VP to the antisense strand or internal 2'-*O*-C16 conjugation at sense strand N6 produced robust knockdown in the spinal cord (up to 80% SOD1 mRNA lowering), but only modest knockdown in the brain (up to 50% SOD1 mRNA lowering). The siRNA combining both 5'-VP and 2'-*O*-C16 had the best activity across CNS regions, with up to 90% SOD1 knockdown in the spinal cord and up to 75% in the brain. There was no activity in the rat striatum, liver, and kidney at the tested dose level and time point.

C16 conjugation enables broad and efficient siRNA delivery to the CNS

The CNS is a complex organ system composed of multiple cell types. To understand C16-siRNA uptake and RNAi activity across the major CNS cell types, we designed siRNAs against cell-specific targets uniquely expressed in neurons (MAP2), astrocytes (GFAP), microglia (IBA1), oligodendrocytes (MBP), and

the endothelium / perivascular macrophages (PECAM1) (Supplementary Table 1). Following a single 0.9 mg IT dose in rats, immunohistochemistry (IHC) to detect siRNA revealed widespread drug distribution in neurons and glial cells (Fig. 2a). Dual IHC confirmed cell-specific uptake in neurons, astrocytes, and microglial cells (Fig. 2a). Drug accumulation in oligodendrocytes was below the limit of detection by IHC (data not shown). IHC also revealed siRNA in vascular endothelium and perivascular macrophages (data not shown), which was shown to be nonfunctional by RT-qPCR (Fig. 2b). Consistent with positive siRNA IHC results, robust knockdown by RT-qPCR was observed in neurons, astrocytes, and microglia (Fig. 2b). There was less effective knockdown in oligodendrocytes, consistent with sub-IHC detection levels. Overall, these data indicate that C16-siRNAs are productively taken up by most CNS cell types of therapeutic relevance.

We then evaluated the dose response and duration of silencing in the rat CNS after a single IT dose of the ESC SOD1-targeting C16-siRNA. At one month post a single IT dose of 0.07 mg, 0.3 mg, or 0.9 mg, dose dependent SOD1 knockdown was observed in the spinal cord and the brain (Fig. 2c). At the lowest dose of 0.07 mg, the knockdown ranged from 20% in the frontal cortex to 50-60% in the thoracic spinal cord and cerebellum. At the highest dose of 0.9 mg, >85% SOD1 knockdown was observed across all CNS regions evaluated. The duration of knockdown was assessed in a six-month study in rats following a single 0.9 mg IT dose. Animals were sacrificed at select time points and SOD1 mRNA knockdown was evaluated across various regions of the CNS and periphery (Fig. 2d). In the lower spinal cord, the maximal level of target knockdown was observed as early as one week post-dose (earliest time point tested), with sustained silencing out to six months. Brain regions showed >75% silencing for at least three months with partial recovery out to six months, except for temporal cortex where SOD1 knockdown started to recover at two months post-dose. Only minimal SOD1 knockdown was detected in liver or kidney under these conditions. One additional cohort of rats received repeat doses of 0.3 mg at approximately monthly intervals for up to five doses, with the last group sacrificed at two weeks post-last dose (4.5 months after the first dose) (Fig. 2e). Silencing appeared to be additive with 88%, 85%, and 81% silencing observed in frontal cortex, cerebellum, and thoracic spinal cord, respectively, at 1 month after three 0.3 mg doses, compared to 85%, 82%, and 82% in those regions at the same time point following a single 0.9 mg dose (Fig. 2d). By 4.5 months, silencing was not substantially changed with 77%, 88%, 93% observed in frontal cortex, cerebellum, and thoracic spinal cord, respectively.

Dose dependent silencing in the frontal cortex corresponded with drug exposure through the 0.07 mg, 0.3 mg, and 0.9 mg groups (Fig. 2f), with the siRNA half-life for the 0.9 mg group calculated to be three to four months. Frontal cortex exposure was generally linear with increasing dose at all time points evaluated. Evidence of accumulation was observed in this tissue following repeat doses, with the siRNA exposure following the third monthly 0.3 mg dose similar to a single 0.9 mg dose, and additive accumulation observed following the fourth and fifth doses. The dose-exposure relationship of the SOD1 C16-siRNA could be characterized across all dose levels explored with a first-order pharmacokinetic model.

To understand the translation of siRNA design requirements for CNS activity from rodents to NHPs, we utilized an Amyloid Precursor Protein (APP)-targeting siRNA with the Enhanced Stabilization Chemistry Plus (ESC+) design (Supplementary Table 1). Following a single IT dose of 60 mg, an unconjugated siRNA lacking 2'-*O*-C16 as well as 5'-VP had minimal activity in the spinal cord and no activity in the brain at three months post-dose (Fig. 3a). Addition of 5'-VP to the antisense strand or internal 2'-*O*-C16 conjugation at N6 of the sense strand produced knockdown in the spinal cord (up to 60% APP lowering), but only modest activity in the brain (up to 30% APP lowering) at three months post-dose. Consistent with the rat data, siRNA containing both 5'-VP and 2'-*O*-C16 had the best activity across CNS regions, with up to 70% APP knockdown in the spinal cord and up to 80% in the brain, including 25% knockdown in deep brain (striatum). There was no activity in NHP liver or kidney at three months post-60 mg IT dose.

We then evaluated the duration of silencing in the NHP after a single IT dose of 60 mg by analyzing serially collected CSF samples utilizing soluble APPα and soluble APPβ biomarker assays (Fig. 3b). Nadir of knockdown was observed as early as one week post-dose (earliest time point tested), with sustained >75% APP silencing for three months post-dose. APP knockdown recovered to 50% at 4.5 months, with full recovery at nine months in most animals as assessed by CSF protein biomarkers.

The relationship of APP silencing in CNS tissues to exposure was evaluated in samples from animals in Figs. 3a and 3b, as well as a third cohort of animals that was sacrificed at approximately 4.5 months following a single 45 mg dose of C16-siRNA. The range of exposures in frontal cortex and thoracic spinal cord from <1 µg/g to approximately 9 µg/g in these animals (Fig. 3c) largely reflects variability in the success of the IT administration, as has be previously noted for ASO[32], rather that nominal dose. Fortuitously, the variability in delivery allowed us to observe a robust exposure response relationship, which was conserved across these tissues. Notably, higher concentrations of C16-siRNA and greater silencing were observed in prefrontal cortex and thoracic spinal cord than in the deep brain region of the striatum.

To evaluate tolerability and safety in NHP CNS, histopathological evaluation of brain, spinal cord, and dorsal root ganglia was performed following terminal necropsy procedures at either three, six, or nine months following a single IT dose of up to 60 mg of the APP-targeting siRNAs (Supplementary Table 1). APP siRNAs, with or without 5'-VP on the antisense strand and/or sense N6 2'-*O*-C16 conjugation, were well-tolerated and there were no test item-related microscopic findings in the examined brain, spinal cord, and dorsal root ganglia sections. Microscopic findings noted were limited to experimental (IT bolus administration in lumbar region and/or CSF collection from cisterna magna) procedure-related changes and consisted of minimal to mild degeneration of nerve fibers localized to the white matter in either the spinal cord (cervical, thoracic, and lumbar segments) and/or brainstem (medulla oblongata region adjacent to aqueduct and underlying pons). Within the affected areas, there were minimal decreases in Luxol Fast Blue (LFB) staining intensity and a minimal increase in the number of IBA-1 positive microglia. Although no concurrent vehicle controls were tested, this assessment was based on similarities with findings reported in NHP and other species following IT administration of vehicle control via implanted

catheters[33], and was further supported by historical control data from similarly executed IT studies in NHP at Contract Research Organizations (Charles River Laboratories and LabCorp).

C16 conjugation enables efficient siRNA delivery to the eye

To assess potency and durability of these novel lipophilic conjugates in NHP eyes, we designed a Transthyretin (TTR)-targeting ESC siRNA containing 2'-*O*-C16 at N6 of the sense strand and 5'-VP on the antisense strand (Supplementary Table 1). A single IVT dose of this siRNA showed dose-dependent lowering of TTR in the aqueous humor, with sustained >80% knockdown out to six months at the dose of 100 or 300 µg/eye (Fig. 4a). At the lowest dose tested (3 µg/eye), TTR protein levels remained reduced by 77% at one month post-dose. To evaluate target engagement in the cells of interest, retinal pigmented epithelium (RPE) was micro-dissected and TTR mRNA levels were measured at six months post-dose relative to control PBS treatment (Fig. 4b). Dose-dependent TTR mRNA lowering was observed, with ~40% knockdown at 3 µg/eye, ~60% knockdown at 30 µg/eye, and >95% knockdown at 100 and 300 µg/eye. TTR protein knockdown in RPE cells was further confirmed by TTR IHC at six months post-dose (Fig. 4c). Finally, to assess the effect of 2'-*O*-C16, we evaluated the activity of an unconjugated version of the TTR siRNA at 10 and 30 µg/eye out to three months post-dose. At one month, aqueous humor TTR protein levels in animals treated with the unconjugated siRNA showed no knockdown at the 10 µg/eye dose and a modest 33% knockdown at the 30 µg/eye dose, compared to 81% knockdown observed for the 2'-*O*-C16 conjugate at 10 µg/eye (Fig. 4d). At three months post-dose, TTR lowering was only observed with the conjugated siRNA.

C16 conjugation enables efficient siRNA delivery to the lung

We also evaluated ESC C16-siRNA distribution and activity in mouse lung following IN administration. IHC to detect administered siRNA was performed on tissue ten days post 10 mg/kg IN dose of the SOD1-targeting C16-siRNA (Fig. 5a) or 28 days post 30 mg/kg IN dose of TRAF6-targeting C16-siRNA (Fig. 5b; Supplementary Table 1). siRNA distributed throughout the whole lung with the greatest accumulation near the mainstem bronchi (Fig. 5a). Closer evaluation showed robust bronchiolar and alveolar uptake (Fig. 5b). The siRNA distribution correlated well with RNAi activity assessed by in situ hybridization (ISH) of the SOD1 target mRNA (Fig. 5c). We were not able to assess activity in the alveoli since SOD1 is only expressed in large airways. To clarify the dose response and time course of silencing, we quantified by RT-qPCR the levels of SOD1 mRNA from homogenized whole lung tissue on 1, 3, 10, 28 and 56 days post a single 10 mg/kg IN dose of the SOD1 C16-siRNA (Fig. 5d). SOD1 mRNA in lung was reduced by 62%-78% in the first month, with sustained activity out to two months post-dose with 57% mRNA lowering. Doses of 0.3, 1, 3, or 10 mg/kg by IN injection resulted in SOD1 mRNA reductions of 57%, 53%, 71%, and 68%, respectively, while a single intravenous (IV) injection at 30 mg/kg reduced SOD1 mRNA by

42% at the same day ten timepoint (Fig. 5e). These data indicate a clear benefit of intranasal delivery of the C16-siRNA to the lungs.

Discussion

Systematic efforts to optimize RNAi therapeutics for potent, durable, and safe silencing of disease-causing gene transcripts in the liver[9,10,34] provided the framework for designing siRNAs for extrahepatic applications. Similar to liver, siRNAs stabilized with 2'-fluoro, 2'-*O*-methyl, and limited terminal phosphorothioate modifications yield robust and durable activity in rodent and NHP CNS, eye, and lung after conjugation with 2'-*O*-C16. The placement of 5'-VP as a stable 5'-phosphate mimic was found to provide an additional boost in activity. The sustained knockdown observed may allow for bi-annual or even less frequent dosing of C16-siRNAs in humans, which is an important consideration due to the challenging nature of IT or IVT dosing. Additionally, off-target mitigation strategies involving placing a thermally destabilizing modification such as GNA in the antisense strand seed region[10] also performed well, thus allowing for translation of safety improvements with the ESC+ platform beyond liver.

Lipophilic ligands, primarily cholesterol, have been widely used to facilitate systemic and local siRNA delivery into extrahepatic organs when conjugated via a linker to the 5'- or 3'-ends of the siRNA[29,35-38]. Cholesterol has been reported to promote local delivery to the eye[39] , lung[36], and CNS[18,27,40], albeit with limited distribution beyond the injection site and, in certain cases, an unacceptable safety profile[17]. Here we report for the first time a systematic evaluation of lipophiles of varying lengths and siRNA design features to identify an optimal conjugate with 2'-*O*-C16 that enables widespread siRNA distribution in the spinal cord and brain following administration into rodent and NHP CSF via a clinically feasible IT dosing route, with no safety signals observed in our studies. The same conjugation strategy also enables broad siRNA distribution and durable activity in the eye and lung after local delivery. The precise mechanisms whereby 2'-*O*-C16 promotes intracellular delivery is currently under investigation but we hypothesize that it promotes 'shuttle-like' moderate affinity interactions with cell membrane and membrane proteins, thus allowing uptake in various cell types. Additionally, the 2'-*O*-C16 ligand may be important for biodistribution and tissue penetration in the CNS as siRNAs lacking 2'-*O*-C16 are functionally taken up near the injection site but do not disperse broadly into CNS parenchyma (data not shown).

While C16-siRNAs provide potent and durable silencing, only a small fraction (< 5%) is retained in the CNS following IT administration (data not shown) and CNS delivery of siRNAs may be further improved by utilizing conjugates with receptor-specific targeting ligands similar to the GalNAc / Asialoglycoprotein Receptor approach for liver. The ultimate solution for patients would be to develop strategies for functional siRNA delivery across the blood brain barrier after systemic administration. With recent encouraging antibody and protein data[41,42], including human proof of concept, it is conceivable that siRNAs may be amenable to the blood brain barrier delivery approach as well. The first C16-siRNA targeting APP is currently in nonclinical development for the treatment of early onset Alzheimer's disease and cerebral amyloid angiopathy.

Materials And Methods

Care and use of laboratory animals

All studies were conducted using protocols consistent with local, state and federal regulations, as applicable, and approved by the Institutional Animal Care and Use Committee (IACUC) at Alnylam Pharmaceuticals, Charles River Laboratories (CRL), or LabCorp (formerly Covance, Inc.), as applicable.

Oligonucleotide synthesis

All oligonucleotides were synthesized on an MerMade 192 or MerMade 12 synthesizer according to previously published protocols[30,43]. 5'-*O*-(4,4'-Dimethoxytrityl)-2'-deoxy-2'-fluoro- and 5'-*O*-(4,4'-dimethoxytrityl)-2'-*O*-methyl-3'-*O*-(2-cyanoethyl-*N*,*N*-diisopropyl) phosphoramidite monomers of uridine, 4-*N*-acetylcytidine, 6-*N*-benzoyladenosine and 2-*N*-isobutyrylguanosine were purchased commercially and (*S*)-GNA phosphoramidites were synthesized according to previously published protocols[44-46]. 2'-*O*-C16 phosphoramidites[47] were used at a concentration of 100-150 mM in acetonitrile with no other changes to synthetic protocols. Phosphorothioate linkages were introduced by sulfurization of phosphite linkages utilizing 0.1 M 3-((*N*,*N*-dimethyl-aminomethylidene)amino)-3*H*-1, 2, 4-dithiazole-5-thione (DDTT) in pyridine. After completion of the solid-phase synthesis, the solid support was incubated in a sealed container with aqueous ammonium hydroxide (28-30%) with added 5% diethylamine by volume, with shaking overnight at 35° C, following a procedure optimized for 5'-(*E*)-vinyl phosphonate oligonucleotide deprotection[48]. The oligonucleotide was filtered to remove the support with 5x volume of water and analyzed by LC-MS and ion-exchange HPLC.

After deprotection and crude quality confirmation, ion-exchange HPLC purification was performed. Purification buffer A consisted of 20 mM sodium phosphate, 15% ACN, pH 8.5. Buffer B was the same composition with an additional 1 M sodium bromide. TSKgel Super Q-5PW (20) anion exchange resin (Tosoh Corporation, 0018546) was used for purification, and a general purification gradient of 15% to 48% in about 20 column volumes was applied. Fractions were analyzed by ion-exchange analysis using a Dionex DNAPac PA200 ion-exchange analytical column, 4mm x 250mm (ThermoFisher, 063000) at room temperature. Buffer A consisted of 20 mM sodium phosphate, 15% acetonitrile, pH 12. Buffer B was identical with additional 1 M sodium bromide. A gradient of 30% to 50% over 12 min with a flow rate of 1 mL/min was used to analyze fractions. Fractions with greater than 85% purity were pooled, concentrated, and desalted over size exclusion columns (GE Healthcare,17-5087-01) with a flow rate of 10 mL/min. All oligonucleotides were purified and desalted, and further annealed to form siRNAs duplexes as previously described[12]. All siRNAs were synthesized by Alnylam Pharmaceuticals (Cambridge, MA).

The identities and purities of all oligonucleotides were confirmed using ESI-LC/MS and IEX HPLC, respectively.

In vitro screening

Rat RPE-J cells (ATCC, CRL-2240) were transfected by adding 0.1 µL of RNAiMAX (Invitrogen, 13778) diluted in 4.9 µL of Opti-MEM to 5 µL of siRNA in a 384-well plate. After a 15 min room temperature incubation, 40 µL of media containing ~5 x10^3 cells was added to the wells. Cells were incubated for 24 hours, and RNA was isolated using an automated protocol on a BioTek-EL406 platform using Dynabeads™ mRNA DIRECT™ Purification Kit (Invitrogen, 61012) according to the manufacturer's instructions. Briefly, 70 µL of Lysis/Binding Buffer and 10 µL of Lysis Buffer containing 3 µL of magnetic beads were added to the plate with cells. Plates were incubated on an electromagnetic shaker for 10 minutes at room temperature. Bead-bound RNA was then washed two times with 150 µL Wash Buffer A and once with Wash Buffer B utilizing magnetic beads. RNA was eluted with 150 µL Elution Buffer.

Complementary DNA (cDNA) synthesis was performed using High-Capacity cDNA Reverse Transcription Kit (Applied Biosystems, 4368813) according to the manufacturer's instructions. Briefly, 10 µL of a master mix containing 1 µL 10X Buffer, 0.4 µL 25X dNTPs, 1 µL 10x random primers, 0.5 µL Reverse Transcriptase, 0.5 µL RNase inhibitor and 6.6 µL water per reaction was added to isolated RNA. Plates were sealed, mixed, and incubated on an electromagnetic shaker for 10 min at room temperature, followed by a 2 hour incubation at 37 °C. 2 µL of cDNA were added to a master mix containing 0.5 µL of rat GAPDH TaqMan probe (Thermo Fisher, 4352338E), 0.5 µL rat SOD1 TaqMan probe (Thermo Fisher, Rn00566938_m1), and 5 µL Lightcycler 480 probe master mix (Roche, 04887301001) per well in a 384-well plate (Roche, 04887301001). Real time quantitative PCR (RT-qPCR) was performed in a LightCycler480 Real Time PCR system (Roche). qPCR data were analyzed using the ΔΔCt method.

Rat IT studies

siRNAs formulated at up to 30 mg/mL in artificial cerebrospinal fluid (aCSF) were administered as 30 µL IT injections by lumbar puncture in the dorsal region of the spine between the L3-L5 vertebral space to male Sprague Dawley rats. At a minimum of 30 minutes prior to surgery, rats were subcutaneously administered 1 mg/kg meloxicam and 0.1 mg/kg buprenorphine. Following anesthesia with isoflurane, rats were placed on a warm heating pad, treated with eye lubricant, and the IT injection site was shaved and disinfected, and an incision was made to expose the spinal column. siRNA was administered with an insulin syringe. Proper placement of the needle was confirmed via CSF backflow in the hub of the needle. Once siRNA administration has been completed, gentle constant pressure on the plunger was maintained for 30 seconds, the incision was sutured and secured with tissue glue, and the rats were placed in sternal recumbency on a heating pad until recovery.

NHP IT studies

siRNAs formulated at 30 mg/mL in aCSF were administered as 2 mL IT injections over 3 minutes by lumbar puncture in the dorsal region of the spine between the L2-L3, L3-L4, L4-L5, or L5-L6 vertebral space of cynomolgus monkeys. Anesthesia was induced with dexmedetomidine and ketamine, and was maintained with supplemental isoflurane as needed. Proper placement of the needle was confirmed via CSF backflow in the hub of the needle. A total volume of 1 mL of CSF was removed prior to dosing, and 0.3 mL aCSF flush was performed following siRNA administration. After completion of the flush, the syringe and needle were removed, and pressure was be applied to injection site for at least 30 seconds, and the animals were allowed to recover. Dexmedetomidine was reversed with atipamezole, as necessary. Serial CSF collections were performed from cisterna magna following procedural anesthesia induced with dexmedetomidine and ketamine and maintained with supplemental isoflurane as needed.

NHP IVT studies

A topical antibiotic (tobramycin) was applied to both eyes twice on the day before and twice on the day after IVT injection to cynomolgus monkeys. The animals received an intramuscular injection of a sedative cocktail (ketamine 5 mg/kg; dexmetedomidine 0.01 mg/kg) followed by isoflurane/oxygen mix through a mask, if deemed necessary to maintain anesthesia. Either 1x phosphate-buffered saline (PBS) or siRNA formulated in 1x PBS were administered in both eyes by IVT injection using a 1 mL syringe and a 30-gauge, ½-inch needle. The dose volume administered was 50 µL/eye. Intravitreal injections were performed by a board-certified veterinary ophthalmologist. Following completion of the dosing procedure, animals received an intramuscular injection of 0.1 mg/kg atipamezole, a reversal agent for dexmetedomidine, as considered necessary. The conjunctivae were flushed with diluted benzalkonium chloride (Zephiran™). Mydriatic drops were be applied to each eye needed.

Mouse IN studies

Female C57BL/6 mice (8-10 weeks of age) were dosed via intranasal instillation (50 µL total, 25 µL/nostril) at the indicated siRNA concentration diluted in 1x PBS and were sacrificed at the indicated day.

RNA extraction and RT-qPCR

For the extraction of RNA, powdered tissues (~10 mg) were resuspended in 700 µL QIAzol and homogenized by vigorous pipetting. Alternatively, two 5 mm steel grinding balls were added to each sample, followed by homogenization at 25/s for 1 min at 4 °C using TissueLyser II (Qiagen, 85300).

Samples were incubated at room temperature for 5 minutes followed by addition of 140 µL chloroform. Samples were mixed by shaking, followed by a 10-minute incubation at room temperature. Samples were spun at 6,000 x g for 15 minutes at 4 °C, the supernatant was transferred to a new tube, and 1.5 volumes of 100% ethanol were added. Samples were then purified using a miRNeasy Kit (Qiagen, 217061) according to the manufacturer's instructions. The RNA was eluted from miRNeasy columns with 50-60 µL RNAse-free water and quantified on a Nanodrop (Thermo Fisher).

Complementary DNA (cDNA) synthesis was performed using High-Capacity cDNA Reverse Transcription Kit (Applied Biosystems, 4368813) according to the manufacturer's instructions. Briefly, 10 µL of a master mix containing 2 µL 10X Buffer, 0.8 µL 25X dNTPs, 2 µL 10X Random Primers, 1 µL MultiScribeTM Reverse Transcriptase, 1 µL RNase Inhibitor, and 3.2 µL of nuclease-free water per reaction was added to 10 µL of the isolated RNA. Plates were incubated in a Thermal Cycler programed for four steps: Step 1 – 25 °C for 10 minutes, Step 2 – 37 °C for 120 minutes, Step 3 – 85 °C for 5 minutes, and Step 4 – hold at 4 °C. qPCR reactions were performed using gene specific TaqMan assays for rat SOD1 (Thermo Fisher, Rn00566938_m1), rat PPIB (Thermo Fisher, Rn03302274_m1), mouse SOD1 (IDT, Mm.PT.58.12368303), mouse GAPDH (Thermo Fisher, Mm99999915_g1), NHP APP (Thermo Fisher, Mf01552283_m1), NHP TTR (Thermo Fisher, Mf02799963_m1), NHP PPIB (Thermo Fisher, Mf02802985_m1), or NHP GAPDH (forward primer: 5'-GCATCCTGGGCTACACTGA-3', reverse primer: 5'-TGGGTGTCGCTGTTGAAGTC-3', probe: 5'HEX-CCAGGTGGTCTCCTCC-3'BHQ-1). qPCR reactions were performed in a Roche LightCycler 480 using LightCycler 480 Probes Master Mix (Roche, 04707494001). qPCR data were analyzed using the ΔΔCt method.

Protein analyses

For sAPP protein analysis in NHP CSF, a V-PLEX panel for sAPPα and sAPPβ (Meso Scale Discovery, K15120E) was used according to the manufacturer's instructions. Briefly, CSF samples were thawed on ice for ~1 hour, followed by centrifugation at 2,000 x g for 5 minutes at 4° C to pellet debris. The resultant supernatant was diluted 1:8 in assay diluent (1% Blocker A in 1X Tris Wash Buffer). Plates were blocked in 3% Blocker A in 1X Tris Wash Buffer for at room temperature for 1 hour on a plate shaker at 600 rpm, and washed 3X with 250 µL 1X Tris Wash Buffer on a ELx405 Biotek plate washer. Samples and calibrators were added to plates and incubated at room temperature for 1 hour on a plate shaker at 600 rpm. Plates were washed 3X with 250 µL 1X Tris Wash Buffer, followed by addition of 1X SULFO-TAG anti-APP detection antibody, and incubated at room temperature for 1 hour on a plate shaker at 600 rpm. Plates were washed 3X with 250 µL 1X Tris Wash Buffer, followed by addition of 150 µL 1X Read Buffer T. Plates were incubated at room temperature for ~10 minutes before reading on a MSD SECTOR Imager Instrument (Meso Scale Discovery).

For TTR protein analysis in NHP aqueous humor, an in-house sandwich ELISA was developed. 96-Well Nunc Maxisorp plates (Invitrogen, 44-2404-21) were coated overnight at 4 °C with Rabbit anti-human TTR pAb (Dako, A0002) at a final concentration of 5.63 µg/ml prepared in 50 mM Carbonate/Bicarbonate

buffer. The following day, plates were washed 5X with 300 µL Tris Buffer containing 0.05% Tween-20 (TBS-T) on a BioTek plate washer. Plates were blocked with 150 µL/well of 1X Powerblock (Biogenex Labs, HK0855K) for 2 hours at room temperature and washed 5X with 300 µL TBS-T. An in-house Cynomolgus TTR standard was used to prepare the highest standard at 59.5 ng/ml, followed by a 2.5-fold dilution series in 1X Powerblock to generate an 8-point standard curve. Aqueous humor samples were tested at a 1:600 dilution in 1X Powerblock. Standards and samples were added to the plate, 100 µL/well, in duplicate and incubated for 2 hours at room temperature with shaking at 600 rpm. Plates were washed 5X with 300 µL TBS-T, followed by addition of secondary antibody, anti-hTTR pAb (Abcam, ab9015), at a final concentration of 4 ug/ml prepared in 1X PowerBlock. Plates were incubated for 1 hour at room temperature with shaking at 600 rpm. Plates were washed 5X with 300 µL TBS-T, and the detection antibody, Donkey anti-sheep pAb Alkaline-Phosphatase, was applied at a final concentration of 1.4 ug/ml in 1X Powerblock (Sigma, A5187). Plates were incubated for 1 hour at room temperature with shaking at 600 rpm. Plates were washed 5X with 300 µL TBS-T, followed by addition of substrate,1.0 mg/ml pNPP (Sigma, N2770). Plates were incubated in the dark at room temperature for ~20 minutes before the addition of 1M Sodium hydroxide to stop the reaction. Absorbance was read at 405 nm on an M5 SpectraMax (Molecular devices). For data analysis, the blank OD units were subtracted from all wells, and the OD units for each calibrator were plotted against the calibrator concentrations and fit with a 4-parameter logistical fit. The concentrations of each replicate of unknowns and the back-calculated concentrations of the standards were interpolated to determine the ng/mL of TTR.

Quantitation of siRNA

Quantitation of siRNAs was performed by liquid chromatography coupled with high resolution mass spectrometry (LC-HRMS), similar to the methods described previously[49,50]. Briefly, tissue samples were homogenized, and tissue homogenates were processed by solid phase extraction using a Clarity OTX 96-well plate (Phenomenex) according to the manufacturer's instructions, and the extracted samples were analyzed by LC-HRMS. The mobile phases used were as follows: mobile phase A: H_2O/HFIP/DIEA (100:1:0.1, v/v/v) with 10 µM EDTA, mobile phase B: H_2O/ACN/HFIP/DIEA (35:65:0.75:0.0375, v/v/v/v) with 10 µM EDTA. The column used was DNAPac RP column (4 µm, 50 x 2.1 mm; Thermo Fisher). Column temperature was set at 90 °C and flow rate was 0.2-0.3 mL/minute. The gradient started with 10% B, progressed to 50% B over 2.5 minutes, and then increased to 100% B in 0.2 minute and maintained for 0.8 minutes; the column was then re-equilibrated with 10% B for 1.5 minutes. A Dionex UltiMate 3000 HPLC system (Thermo Fisher) in combination with an Accela Open Autosampler (Thermo Fisher) and a Q Exactive mass spectrometer (Thermo Fisher) was used for the LC-HRMS analysis. The oligonucleotides were analyzed in negative ionization mode. The mass spectrometer was set at parallel reaction monitoring mode.

Histopathology, IHC, and ISH

All animals were sacrificed in accordance with AVMA Guidelines for the Euthanasia of Animals. Tissues were collected[51] and fixed in 10% neutral-buffered formalin, processed routinely, and stained with hematoxylin and eosin (H&E) as described previously[10]. H&E based microscopic findings were recorded in the Pristima v7.0.0 System (Xybion, NJ) and graded on a scale of 1-5, (1=minimal, 2= mild, 3=moderate, 4=marked, and 5=severe) by a board-certified veterinary pathologist.

Luxol fast blue/cresyl-echt violet (LFB/CEV) stain for myelin was performed on spinal cord, brainstem and cerebellum. Briefly, deparaffinized sections were dehydrated through three changes in xylene, 2 minutes each, and rehydrated through two changes of 100% and 95% ethanol, 2 minutes each. Sections were stained with 0.1 % LFB (StatLab, Columbia, MD) either for 1 hour at 60° C or overnight at room temperature, followed by three to five rinses in 95% ethanol, distilled water, and differentiation in 0.05% lithium carbonate for three to five seconds. Next, sections were rinsed in distilled water followed by counter staining with CEV for 10 minutes, dehydrated through graded alcohols and xylene, and routinely coverslipped. Decreases in LFB staining intensity and increases in IBA1 staining indicative of microgliosis were semi-quantitatively scored on a scale of 1-4 (1=minimal, 2= mild, 3=moderate, and 4=marked).

Immunohistochemistry (IHC) and in-situ hybridization (ISH) were performed on the Discovery Ultra automated instrument (Ventana Medical Systems, Tucson, AZ) using manufacturer-provided reagents and protocols. For IHC, antibodies against the following targets were used: IBA1 1:1600 (#019-19741, Fujifilm Wako, Richmond, VA), GFAP 1:4000 (#Z0334, Agilent-Dako, Santa Clara, CA), CD31 1:75 (#ab23874, Abcam, Waltham, MA), MAP2 1:1000 (#ab5392, Abcam), TTR 1:800 (prealbumin, #SC-8104, Santa Cruz Biotechnology, Dallas, TX), and in-house anti-siRNA rabbit polyclonal antibody ab19151 at 1:12000. IBA1, GFAP, and CD31 were detected with anti-rabbit NP multimer followed by anti-NP AP multimer and Discovery Yellow AP Chromagen (all Ventana). MAP2 was detected with goat anti-chicken antibody (#6100-08, Southern Biotech, Birmingham, AL), followed by anti-goat HRP secondary antibody and Discovery Green HRP Chromogen (both Ventana). TTR was detected by anti-goat HRP secondary antibody followed by Discovery Purple HRP Chromogen (both Ventana). siRNA was detected with anti-rabbit HRP secondary antibody followed by Discovery Purple HRP Chromogen (Ventana). For ISH, sections were hybridized with a SOD1 mRNA probe (Advanced Cell Diagnostics, 428589) followed by detection with RNAScope DAB amplification kit (Advanced Cell Diagnostics, 323200) and visualization with mRNA DAB Chromogen (Ventana).

Declarations

Acknowledgements

The authors thank Alnylam's Medicinal Chemistry Team, Medium Scale Synthesis Team, High Throughput Synthesis Team, and Duplex Annealing Team for siRNA synthesis; Anna Bisbe, Patrick Miller and Ryan Malone for siRNA purification, Catrina Wong, Shirley Maczko, Martha Mendez, Irma Duarte and

Dina Rooney for in vivo study support; Amy Guan for tissue processing; Julia Varao for sample management; Ben Fitzsimmons for tissue drug concentration analysis; Brenda Carito, Paul Gedman, and Kelsey Bittner for histology support; and Alnylam's Research Analytical Team for metabolic stability studies.

Competing Financial Interests

The authors declare competing financial interests: details are available in the online version of the paper. All authors are employees of Alnylam Pharmaceuticals with salary and stock options.

Data Availability Statement

The datasets generated during and/or analysed during the current study are available from the corresponding author on reasonable request.

References

1. Setten, R.L., Rossi, J.J. & Han, S.P. The current state and future directions of RNAi-based therapeutics. *Nat Rev Drug Discov* **18**, 421-446 (2019).

2. Adams, D. et al. Patisiran, an RNAi Therapeutic, for Hereditary Transthyretin Amyloidosis. *N Engl J Med* **379**, 11-21 (2018).

3. Kristen, A.V. et al. Patisiran, an RNAi therapeutic for the treatment of hereditary transthyretin-mediated amyloidosis. *Neurodegener Dis Manag* **9**, 5-23 (2019).

4. Balwani, M. et al. Phase 3 Trial of RNAi Therapeutic Givosiran for Acute Intermittent Porphyria. *N Engl J Med* **382**, 2289-2301 (2020).

5. Garrelfs, S.F. et al. Lumasiran, an RNAi Therapeutic for Primary Hyperoxaluria Type 1. *N Engl J Med* **384**, 1216-1226 (2021).

6. Raal, F.J. et al. Inclisiran for the Treatment of Heterozygous Familial Hypercholesterolemia. *N Engl J Med* **382**, 1520-1530 (2020).

7. Ray, K.K. et al. Inclisiran in Patients at High Cardiovascular Risk with Elevated LDL Cholesterol. *N Engl J Med* **376**, 1430-1440 (2017).

8. Ray, K.K. et al. Two Phase 3 Trials of Inclisiran in Patients with Elevated LDL Cholesterol. *N Engl J Med* **382**, 1507-1519 (2020).

9. Foster, D.J. et al. Advanced siRNA Designs Further Improve In Vivo Performance of GalNAc-siRNA Conjugates. *Mol Ther* **26**, 708-717 (2018).

10. Janas, M.M. et al. Selection of GalNAc-conjugated siRNAs with limited off-target-driven rat hepatotoxicity. *Nat Commun* **9**, 723 (2018).

11. Nair, J.K. et al. Impact of enhanced metabolic stability on pharmacokinetics and pharmacodynamics of GalNAc-siRNA conjugates. *Nucleic Acids Res* **45**, 10969-10977 (2017).

12. Nair, J.K. et al. Multivalent N-acetylgalactosamine-conjugated siRNA localizes in hepatocytes and elicits robust RNAi-mediated gene silencing. *J Am Chem Soc* **136**, 16958-61 (2014).

13. Finkel, R.S. et al. Nusinersen versus Sham Control in Infantile-Onset Spinal Muscular Atrophy. *N Engl J Med* **377**, 1723-1732 (2017).

14. Dorn, G. et al. siRNA relieves chronic neuropathic pain. *Nucleic Acids Res* **32**, e49 (2004).

15. Miller, V.M. et al. Allele-specific silencing of dominant disease genes. *Proc Natl Acad Sci U S A* **100**, 7195-200 (2003).

16. Pomerantz, R.J. RNA interference:a potential novel therapeutic combating HIV-1 in the central nervous system. *Arch Immunol Ther Exp (Warsz)* **52**, 401-9 (2004).

17. Nikan, M. et al. Docosahexaenoic Acid Conjugation Enhances Distribution and Safety of siRNA upon Local Administration in Mouse Brain. *Mol Ther Nucleic Acids* **5**, e344 (2016).

18. Alterman, J.F. et al. Hydrophobically Modified siRNAs Silence Huntingtin mRNA in Primary Neurons and Mouse Brain. *Mol Ther Nucleic Acids* **4**, e266 (2015).

19. Alterman, J.F. et al. A divalent siRNA chemical scaffold for potent and sustained modulation of gene expression throughout the central nervous system. *Nat Biotechnol* **37**, 884-894 (2019).

20. Zhou, Y. et al. Blood-brain barrier-penetrating siRNA nanomedicine for Alzheimer's disease therapy. *Sci Adv* **6**(2020).

21. Gregory, J.V. et al. Systemic brain tumor delivery of synthetic protein nanoparticles for glioblastoma therapy. *Nat Commun* **11**, 5687 (2020).

22. Eyford, B.A. et al. A Nanomule Peptide Carrier Delivers siRNA Across the Intact Blood-Brain Barrier to Attenuate Ischemic Stroke. *Front Mol Biosci* **8**, 611367 (2021).

23. Gupta, A., Kafetzis, K.N., Tagalakis, A.D. & Yu-Wai-Man, C. RNA therapeutics in ophthalmology - translation to clinical trials. *Exp Eye Res* **205**, 108482 (2021).

24. DeVincenzo, J. et al. A randomized, double-blind, placebo-controlled study of an RNAi-based therapy directed against respiratory syncytial virus. *Proc Natl Acad Sci U S A* **107**, 8800-5 (2010).

25. https://ir.arrowheadpharma.com/static-files/838140be-e2bb-4cdb-a1cc-97d3a154ca80.

26. https://www.atsjournals.org/doi/abs/10.1164/ajrccm-conference.2019.199.1_MeetingAbstracts.A5391.

27. Chen, Q. et al. Lipophilic siRNAs mediate efficient gene silencing in oligodendrocytes with direct CNS delivery. *J Control Release* **144**, 227-32 (2010).

28. Manoharan, M. Oligonucleotide conjugates as potential antisense drugs with improved uptake, biodistribution, targeted delivery, and mechanism of action. *Antisense Nucleic Acid Drug Dev* **12**, 103-28 (2002).

29. Wolfrum, C. et al. Mechanisms and optimization of in vivo delivery of lipophilic siRNAs. *Nat Biotechnol* **25**, 1149-57 (2007).

30. Schlegel, M.K. et al. Chirality Dependent Potency Enhancement and Structural Impact of Glycol Nucleic Acid Modification on siRNA. *J Am Chem Soc* **139**, 8537-8546 (2017).

31. Parmar, R. et al. 5'-(E)-Vinylphosphonate: A Stable Phosphate Mimic Can Improve the RNAi Activity of siRNA-GalNAc Conjugates. *Chembiochem* **17**, 985-9 (2016).

32. Sullivan, J.M. et al. Convective forces increase rostral delivery of intrathecal radiotracers and antisense oligonucleotides in the cynomolgus monkey nervous system. *J Transl Med* **18**, 309 (2020).

33. Butt, M.T. Morphologic changes associated with intrathecal catheters for direct delivery to the central nervous system in preclinical studies. *Toxicol Pathol* **39**, 213-9 (2011).

34. Janas, M.M. et al. Safety evaluation of 2'-deoxy-2'-fluoro nucleotides in GalNAc-siRNA conjugates. *Nucleic Acids Res* **47**, 3306-3320 (2019).

35. Osborn, M.F. & Khvorova, A. Improving siRNA Delivery In Vivo Through Lipid Conjugation. *Nucleic Acid Ther* **28**, 128-136 (2018).

36. Biscans, A. et al. Diverse lipid conjugates for functional extra-hepatic siRNA delivery in vivo. *Nucleic Acids Res* **47**, 1082-1096 (2019).

37. Raouane, M., Desmaele, D., Urbinati, G., Massaad-Massade, L. & Couvreur, P. Lipid conjugated oligonucleotides: a useful strategy for delivery. *Bioconjug Chem* **23**, 1091-104 (2012).

38. Kubo, T. et al. Palmitic acid-conjugated 21-nucleotide siRNA enhances gene-silencing activity. *Mol Pharm* **8**, 2193-203 (2011).

39. Byrne, M. et al. Novel hydrophobically modified asymmetric RNAi compounds (sd-rxRNA) demonstrate robust efficacy in the eye. *J Ocul Pharmacol Ther* **29**, 855-64 (2013).

40. DiFiglia, M. et al. Therapeutic silencing of mutant huntingtin with siRNA attenuates striatal and cortical neuropathology and behavioral deficits. *Proc Natl Acad Sci U S A* **104**, 17204-9 (2007).

41. Kariolis, M.S. et al. Brain delivery of therapeutic proteins using an Fc fragment blood-brain barrier transport vehicle in mice and monkeys. *Sci Transl Med* **12**(2020).

42. Ullman, J.C. et al. Brain delivery and activity of a lysosomal enzyme using a blood-brain barrier transport vehicle in mice. *Sci Transl Med* **12**(2020).

43. Nair, J.K. et al. Multivalent N-Acetylgalactosamine-Conjugated siRNA Localizes in Hepatocytes and Elicits Robust RNAi-Mediated Gene Silencing. *Journal of the American Chemical Society* **136**, 16958-16961 (2014).

44. Zhang, L., Peritz, A. & Meggers, E. A Simple Glycol Nucleic Acid. *Journal of the American Chemical Society* **127**, 4174-4175 (2005).

45. Zhang, L., Peritz, A.E., Carroll, P.J. & Meggers, E. Synthesis of Glycol Nucleic Acids. *Synthesis* **2006**, 645-653 (2006).

46. Schlegel, M.K. & Meggers, E. Improved Phosphoramidite Building Blocks for the Synthesis of the Simplified Nucleic Acid GNA. *The Journal of Organic Chemistry* **74**, 4615-4618 (2009).

47. WO2019217459.

48. O'Shea, J. et al. An efficient deprotection method for 5'-[O,O-bis(pivaloyloxymethyl)]-(E)-vinylphosphonate containing oligonucleotides. *Tetrahedron* **74**, 6182-6186 (2018).

49. Li, J. et al. Discovery of a novel deaminated metabolite of a single-stranded oligonucleotide in vivo by mass spectrometry. *Bioanalysis* **11**, 1955-1965 (2019).

50. Liu, J. et al. Oligonucleotide quantification and metabolite profiling by high-resolution and accurate mass spectrometry. *Bioanalysis* **11**, 1967-1980 (2019).

51. Bolon, B. et al. STP position paper: Recommended practices for sampling and processing the nervous system (brain, spinal cord, nerve, and eye) during nonclinical general toxicity studies. *Toxicol Pathol* **41**, 1028-48 (2013).

Figures

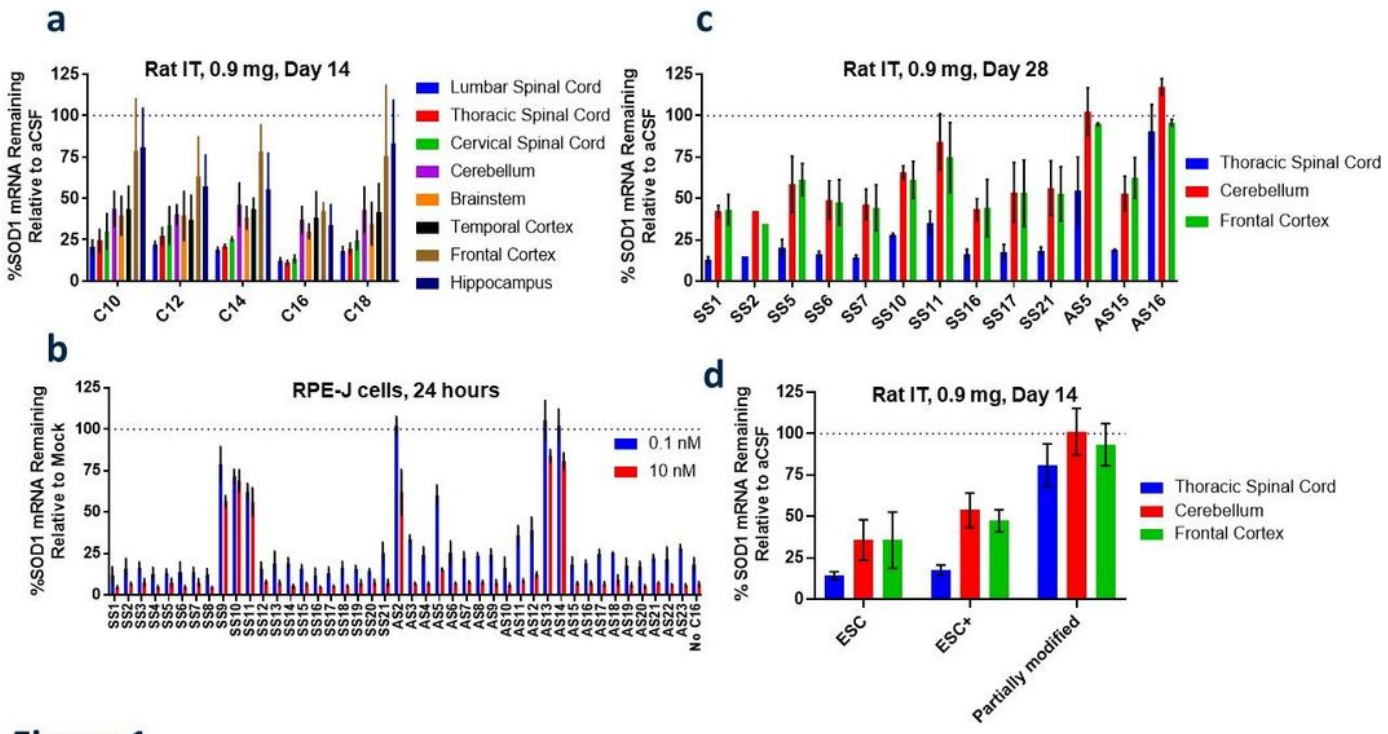

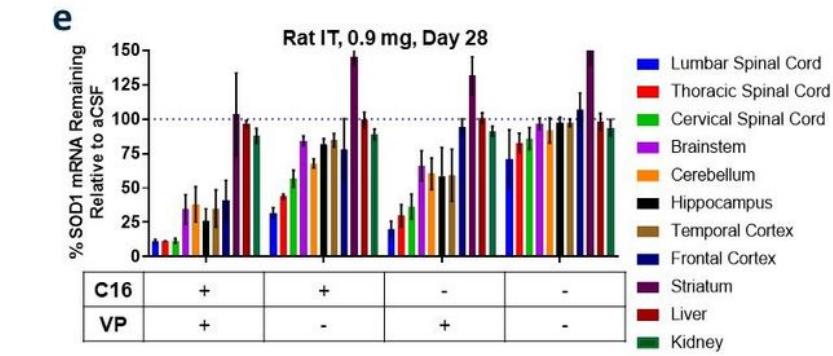

Figure 1

Optimization of the siRNA design for CNS delivery in the rat. (a) 5'-vinylphosphonate (VP)-modified SOD1-targeting siRNA was conjugated to lipids (C10, C12, C14, C16, or C18 oleyl) via 2'-O-position at N6 nucleotide of the sense strand and administered as a single intrathecal (IT) bolus injection to rats at 0.9 mg. Spinal cord and brain regions were collected two weeks post-dose for SOD1 mRNA knockdown measurement by RT-qPCR normalized to housekeeping PPIB mRNA relative to artificial CSF (aCSF)-dosed

animals. N=4 per group. (b) 2'-O-C16 modification was conjugated across sense and antisense strands of 5'-VP-modified SOD1-targeting siRNA and transfected into RPE-J cells at 0.1 or 10 nM for potency assessment. After 24 hours, SOD1 mRNA was quantified by RT-qPCR normalized to housekeeping GAPDH mRNA relative to mock transfection. (c) 2'-O-C16 was conjugated at various positions of the sense or antisense strand of 5'-VP-modified SOD1-targeting siRNA and administered as a single IT bolus injection to rats at 0.9 mg. Spinal cord and brain regions were collected one month post-dose for SOD1 mRNA knockdown measurement by RT-qPCR normalized to housekeeping PPIB mRNA relative to aCSF-dosed animals. N=3 per group. (d) Partially or fully modified (ESC, ESC+) 5'-VP-modified SOD1-targeting siRNA (Supplementary Table 1) was conjugated to 2'-O-C16 at N6 of the sense strand and administered as a single IT bolus injection to rats at 0.9 mg. Spinal cord and brain regions were collected two weeks post-dose for SOD1 mRNA knockdown measurement by RT-qPCR normalized to housekeeping PPIB mRNA relative to aCSF-dosed animals. N=2-5 per group. (e) SOD1-targeting siRNA was modified either with VP at the 5' end of the antisense strand, 2'-O-C16 at N6 of the sense strand, or both, and administered as a single IT bolus injection to rats at 0.9 mg. Spinal cord, brain regions, and peripheral organs were collected at one-month post-dose for SOD1 mRNA knockdown measurement by RT-qPCR normalized to housekeeping PPIB mRNA relative to aCSF-dosed animals. N=3 per group. Error bars represent standard deviation.

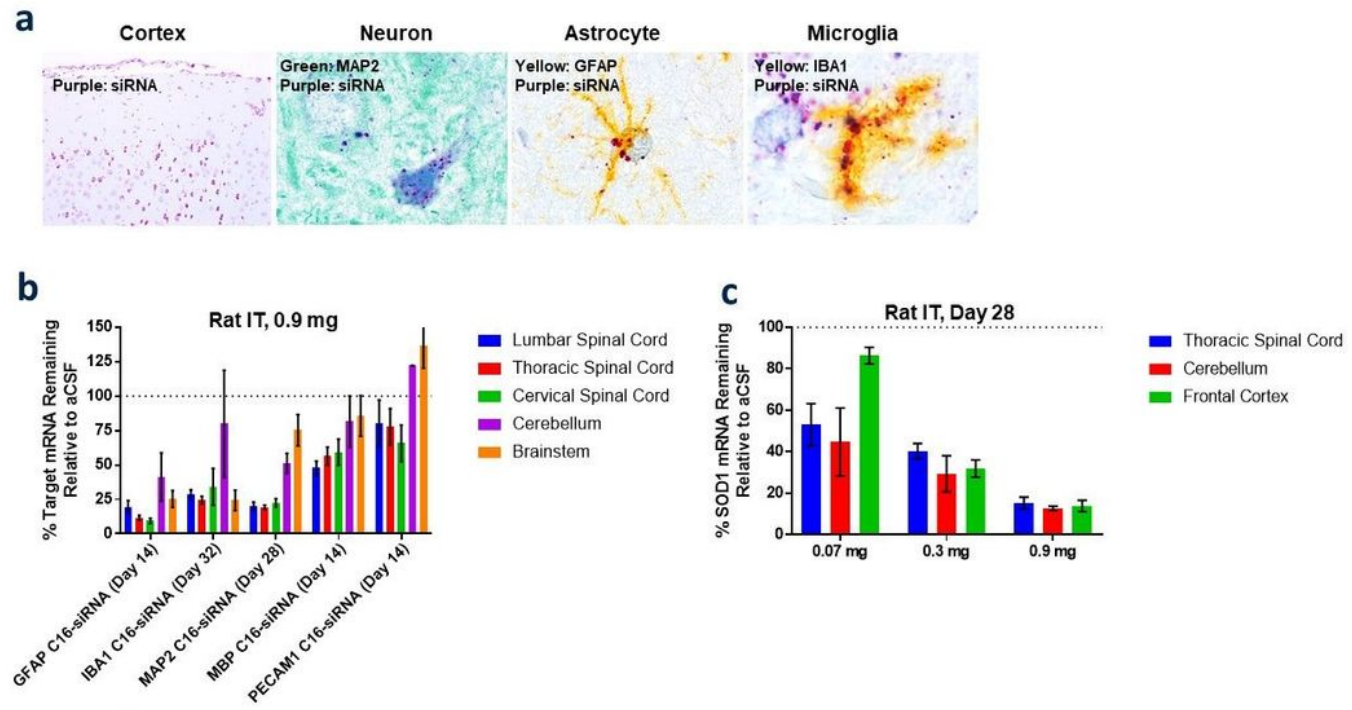

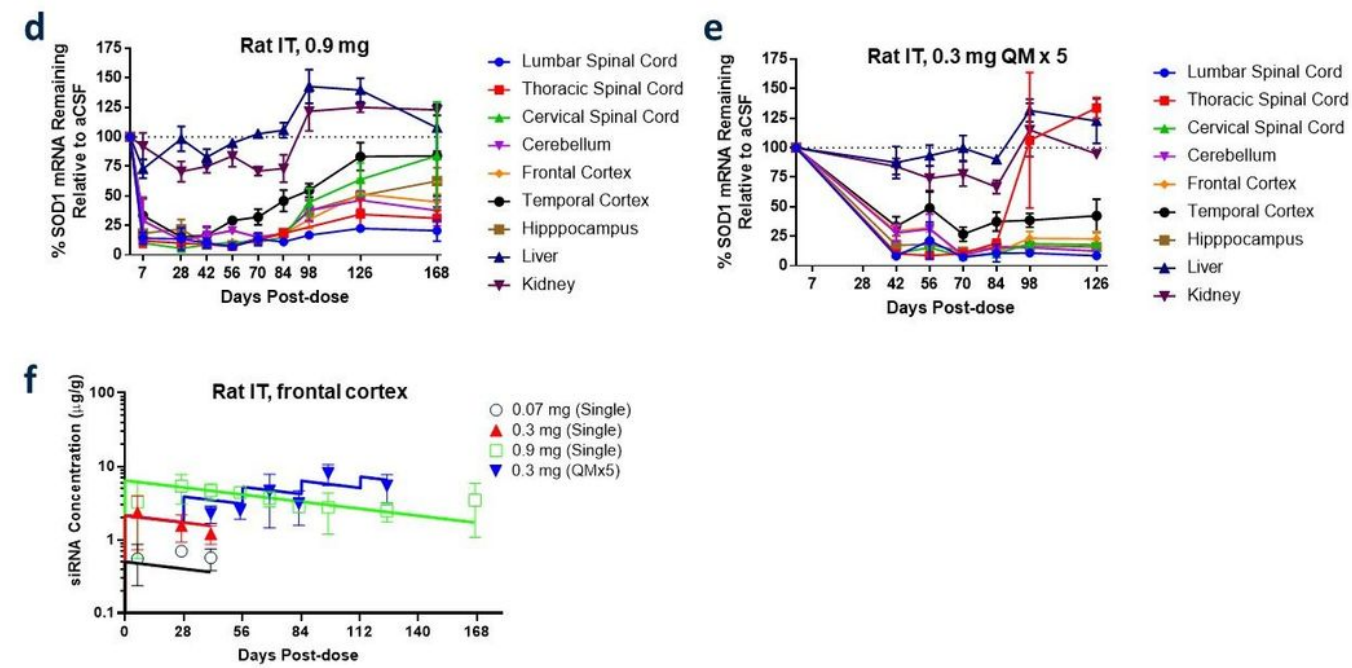

Figure 2

Characterization of the C16-siRNA in rat CNS. (a) siRNA immunohistochemistry (IHC) demonstrated robust neuronal and glial cell drug accumulation (magenta) in cerebral cortex (left panel). Dual IHC localized siRNA in neurons (MAP2), astrocytes (GFAP) and microglia (IBA1). (b) C16-siRNAs targeting CNS cell-type specific transcripts (MAP2 - neurons, GFAP - astrocytes, IBA1 - microglia, MBP - oligodendrocytes, and PECAM1 - endothelium / perivascular macrophages) were administered as a single

intrathecal (IT) bolus injection to rats at 0.9 mg. Spinal cord and brain regions were collected at two weeks post-dose (GFAP, PECAM1, MBP) or one-month post-dose (MAP2, IBA1) for target mRNA knockdown measurement by RT-qPCR normalized to housekeeping PPIB mRNA relative to aCSF-dosed animals. N=2-5 per group. (c) C16-siRNA targeting SOD1 was administered as a single IT bolus injection to rats at 0.07, 0.3 or 0.9 mg. Spinal cord and brain regions were collected at one month post-dose for target mRNA knockdown measurement by RT-qPCR normalized to housekeeping PPIB mRNA relative to aCSF-dosed animals. N=3 per group. (d) C16-siRNA targeting SOD1 was administered as a single IT bolus injection to rats at 0.9 mg. Spinal cord, brain regions, and peripheral organs were collected at indicated days post-dose, out to six months, for target mRNA knockdown measurement by RT-qPCR normalized to housekeeping PPIB mRNA relative to aCSF-dosed animals. N=3 per group. (e) C16-siRNA targeting SOD1 was administered as a monthly IT bolus injection to rats at 0.3 mg for a total of up to five injections over four months. Spinal cord, brain regions, and peripheral organs were collected at indicated days, out to 4.5 months, for target mRNA knockdown measurement by RT-qPCR normalized to housekeeping PPIB mRNA relative to aCSF-dosed animals. N=3 per group. (f) SOD1 C16-siRNA was administered as single IT injections of 0.07, 0.3 or 0.9 mg, or monthly 0.3 mg injections for a total of up to five injections over four months. Frontal cortex concentrations (dots) showed dose-linearity in single-dose escalation study in rats, and additive exposure in multi-dose arm. The straight-forward pharmacokinetics (PK) of C16-siRNA in rat CNS were well-characterized by a first order PK model (solid lines). Error bars represent standard deviation.

Figure 3

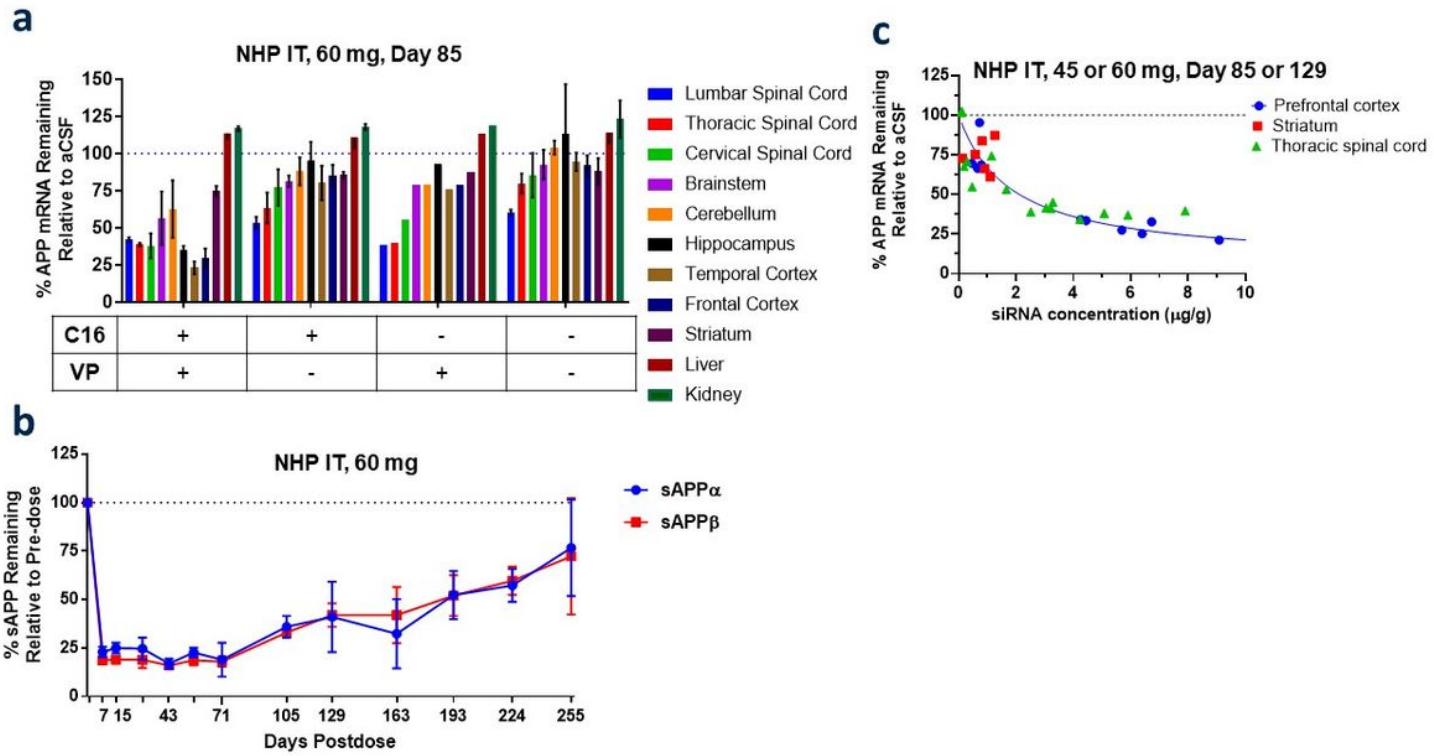

Figure 3

Translation of C16-siRNA activity in nonhuman primate CNS. (a) APP-targeting siRNA was modified either with vinylphosphonate (VP) at the 5' end of the antisense strand, 2'-O-C16 at N6 of the sense strand, or both, and administered as a single intrathecal (IT) bolus injection to cynomolgus monkeys at 60 mg. Spinal cord, brain regions, and peripheral organs were collected at three months post-dose for APP mRNA knockdown measurement by RT-qPCR normalized to housekeeping PPIB mRNA relative to aCSF-dosed animals. N=1-4 per group. (b) C16-siRNA targeting APP was administered as a single IT bolus injection to three cynomolgus monkeys at 60 mg. Cerebrospinal fluid (CSF) was collected at indicated days post-dose, out to nine months, for soluble APPα (sAPPα) and soluble APPβ (sAPPβ) measurement relative to pre-dose. N=3 per group. (c) C16-siRNA concentrations were evaluated in CNS tissue samples obtained from animals from panels (a) and (b), and from a third group of animals (N=3) sacrificed at 4.5 months following a 45 mg nominal dose. Higher concentrations of C16-siRNA targeting APP were observed in the spinal cord and prefrontal cortex comparted to the striatum, though the relationship between drug-exposure and mRNA reduction was similar in each tissue. Error bars represent standard deviation.

Figure 4

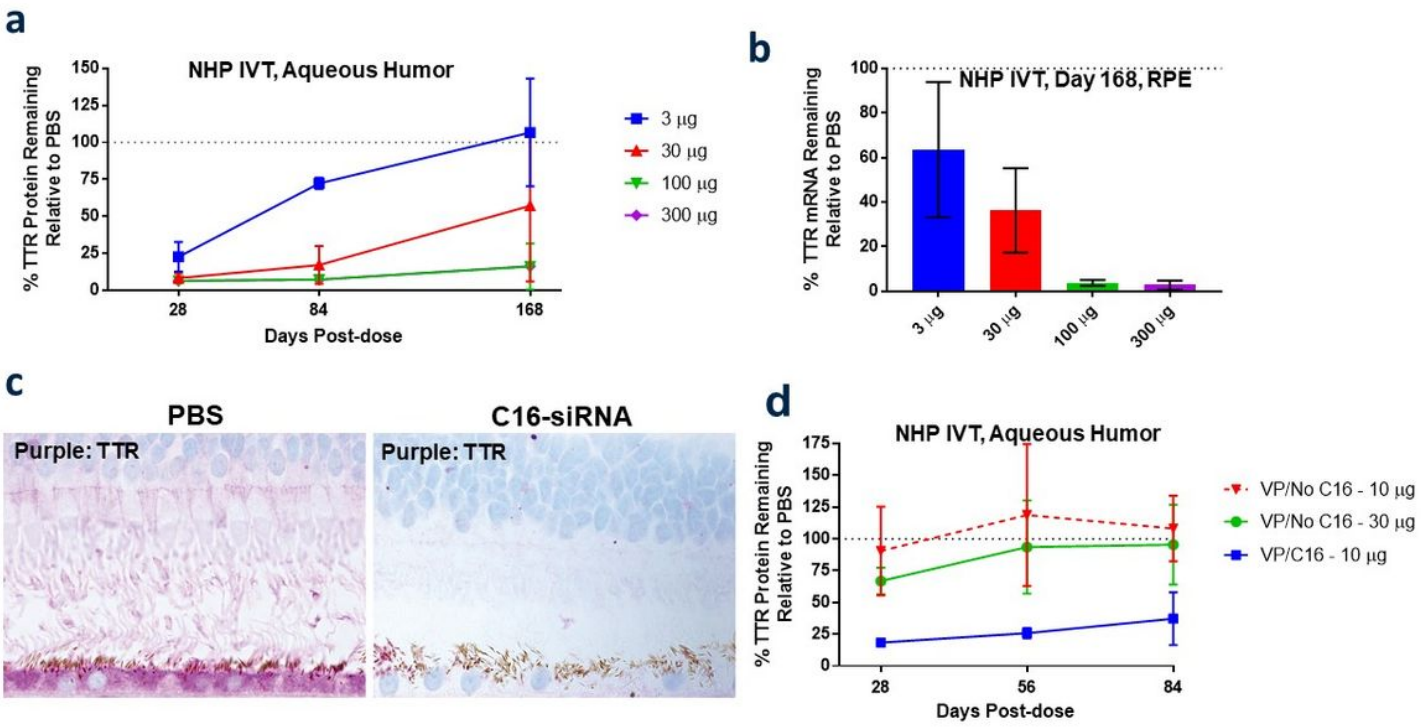

Figure 4

Translation of C16-siRNA activity in nonhuman primate eye. (a) TTR-targeting siRNA with vinylphosphonate (VP) at the 5' end of the antisense strand and 2'-O-C16 at N6 of the sense strand was administered as a single intravitreal (IVT) injection to cynomolgus monkeys at 60 mg at 3, 30, 100 or 300 µg/eye. Aqueous humor was collected at indicated days post-dose, out to six months, for secreted TTR protein measurement relative to PBS-dosed animals. N=4 per group. (b) TTR knockdown was further confirmed on day 168 by TTR mRNA knockdown measurement by RT-qPCR normalized to housekeeping GAPDH mRNA relative to PBS-dosed animals in micro-dissected retinal pigmented epithelium (RPE). N=4

per group. (c) TTR immunohistochemistry (TTR) confirmed protein knockdown in RPE, along with knockdown of secreted protein adherent to photoceptor cells above. (d) Unconjugated TTR-targeting siRNA modified with VP at the 5' end of the antisense strand was dosed IVT in cynomolgus monkeys at 10 and 30 µg/eye and compared to a 10 µg/eye dose of the 2'-O-C16-conjugated version. Aqueous humor was collected at indicated days post-dose, out to three months, for secreted TTR protein measurement relative to PBS-dosed animals. N=4 per group. Error bars represent standard deviation.

Figure 5

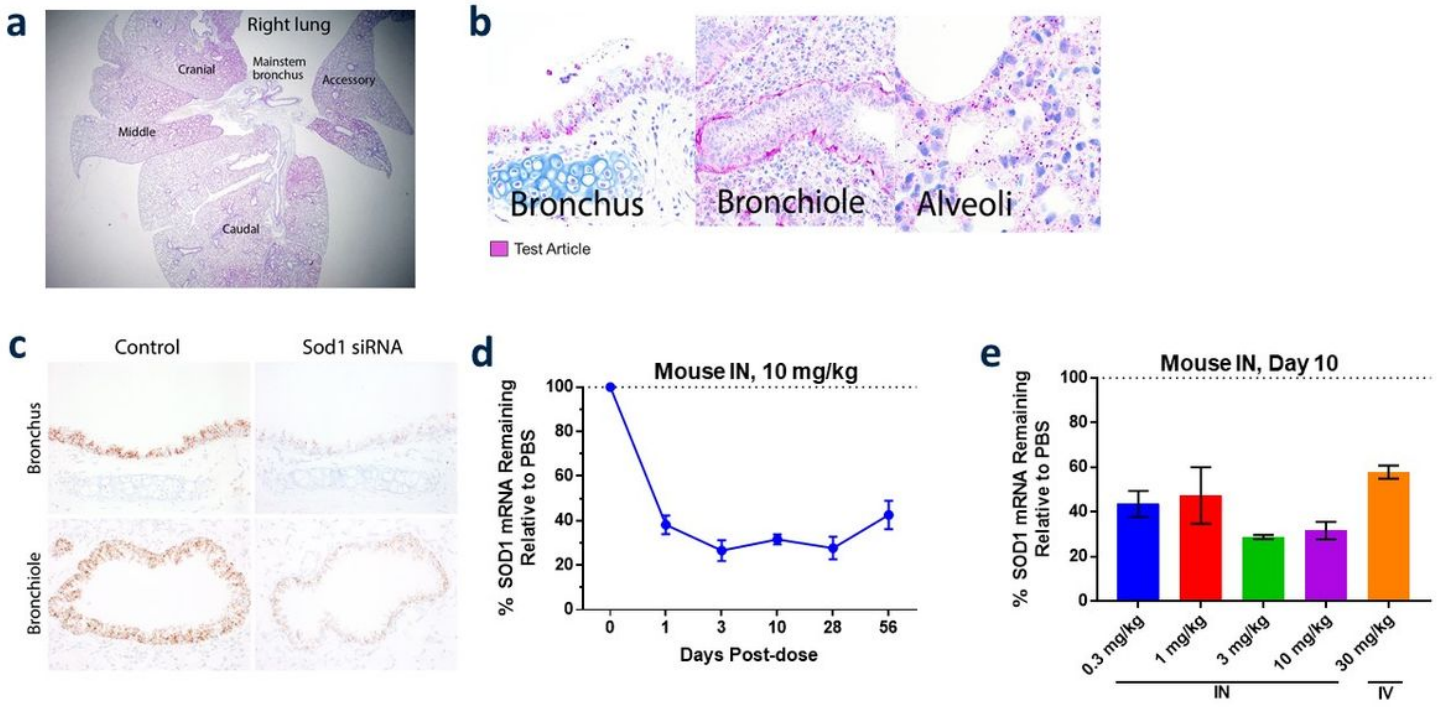

Figure 5

C16-siRNA distribution and activity in mouse lung. (a-b) C16-siRNAs with vinylphosphonate (VP) at the 5' end of the antisense strand and 2'-O-C16 at N6 of the sense strand were administered in mice intranasally (IN) at (a) 10 mg/kg (SOD1) or (b) 30 mg/kg (TRAF6). Lungs were collected on day 10 or 28 post-dose, respectively, for siRNA immunohistochemistry (IHC). siRNA, magenta; hematoxylin counterstain, blue. (c) SOD1 mRNA knockdown was visualized by in situ hybridization (ISH) on day 10 post 10 mg/kg IN dose of SOD1-targeting C16-siRNA. SOD1 mRNA, brown; hematoxylin counterstain, blue. (d) RT-qPCR of SOD1 mRNA in whole lung measured on days 1, 3, 10, 28, 56 post 10 mg/kg IN dose of SOD1-targeting C16-siRNA. N=3 per group. (e) RT-qPCR of SOD1 mRNA in whole lung measured on day 10 after 0.3, 1, 3 or 10 mg/kg single IN dose or 30 mg/kg single intravenous (IV) dose of SOD1-targeting C16-siRNA. N=3 per group. Error bars represent standard deviation.

Supplementary Files

This is a list of supplementary files associated with this preprint. Click to download.

- nreditorialpolicychecklist.pdf
- nrreportingsummary.pdf
- SupplementaryTables.docx